APPLYING CRYSTALLOGRAPHY IN ANALYSIS OF TRABECULAR BONE BACKSCATTER

JANUSZ WOJCIK, JERZY LITNIEWSKI, ANDRZEJ NOWICKI, BARBARA GAMBIN

Institute of the Fundamental Technological Research of the Polish Academy of Sciences
5B, Adolfa Pawińskiego St., 02-106 Warsaw, Poland
jwojcik@ippt.gov.pl

Some important details of the Backscatter Effective Cross-Sections obtained for random scattering structures (like trabecular bone) are explain by comparison with the results obtained by means of the simplified theoretical model. The simplified model was (establish) and justified on the basis of the structural analysis of the results obtained for exact model of the field scattering on complex structures. The simplified model is commonly used in description of the scattering on the regular structures like crystal.

Comparison with experimental results for the trabecular bone is also presented. The results allowed to conclude that crystallographic methods could be potentially useful for extracting characteristic features of trabecular bone.

INTRODUCTION

The ultrasound signals being scattered in trabecular bone contain information on the properties of the bone structure, and hence the analysis of these signals could be useful in assessment of the microscopic architecture of the bone. The Wear's [1] work contains the review of methods and problems of bone sonometry. It has been demonstrated that the use of the backscattering models enabled an assessment of micro structural characteristics from experimental data.

In this approach the model of trabecular bone was proposed that consisted of finite length, elastic, cylindrical elements of varying diameters and orientation. The physical properties of the cylinders were assumed similar to those of a bone tissue. The multi-element structure of the bone model was similar to the architecture of the trabecular bone [2] including statistical variation of trabeculae size and characteristic dimensions of the bone structure.

The field scattered on the bone model was evaluated by solving numerically the integral form of the Sturm-Liouville equation that describes scalar wave in inhomogeneous, attenuating

medium. For the calculated scattered fields the Backscatter Effective Cross-Sections (BECS) coefficient was determined in the frequency range up to 3 MHz.

It was shown that some characteristic dimensions of the structure could be extracted from the backscattered echo signals when analyzing the frequency dependence of the backscattering coefficient. We have found that the monotonic increase of the BECS with frequency was disturbed by characteristic peaks. Existence of BECS peaks for the particular frequencies was explained applying the Laue's equations that state the conditions for incident waves to be diffracted by a crystal lattice [3]. The low frequency peak at 0.75 MHz corresponded to 1 mm mean distance between thick trabeculae and its existence was confirmed experimentally.

We have shown that crystallographic methods could be potentially useful for extracting characteristic features of trabecular bone, despite the fact that analyzed bone structure exhibited features much more randomized than those of the crystals and scattering is an random process.

1. MEDIUM DESCRIPTION AND SCATTERING EQUATIONS

The Lame's equation for longitudinal (volumetric) disturbances in non-homogeneous, isotropic, and stationary medium given in [4] can be generalized for lossy medium and rewritten in space-Fourier frequency domain as Sturm-Liouville equation [5]

$$\begin{gathered}\Delta C + k^2 C = \mathrm{V} C + \mathbf{Q}\cdot\nabla C \\ \mathrm{V} = \mathrm{V}(\mathbf{x},n) \equiv -\left(K(x,n)^2 - k(n)^2\right), \quad \mathbf{Q}(\mathbf{x}) \equiv \nabla g / g \\ K^2 = K(\mathbf{x},n)^2 \equiv \frac{n^2}{c^2\left(1-2i(a(\mathbf{x},n)/gc^2n)\right)}, \quad k^2 = k(n)^2 \equiv \frac{n^2}{\left(1-2i(a_0(n)/n)\right)}\end{gathered} \tag{1}$$

where $C = C(\mathbf{x},n) = F\left[P(\mathbf{x},t)\right]$; $P = P(\mathbf{x},t)$ is the normalized stress; $P \equiv \overline{P}/P_0$, P_0 is the reference pressure; $g = g(\mathbf{x})$, $c = c(\mathbf{x})$ are respectively: normalized density and speed of the longitudinal (sound) waves, $(\mathbf{x},t)$ are normalized coordinates in space and time, whereas ∇ is the normalized nabla vector operator, symbol:• denotes scalar product, $\Delta \equiv \nabla\cdot\nabla$ is the scalar Laplacian. The normalization was performed as follows: $g \equiv \overline{g}/g_0$, $c \equiv \overline{c}/c_0$, $\mathbf{x} \equiv K_0\overline{\mathbf{x}}$, $t \equiv \omega_0\overline{t}$, $\nabla \equiv \overline{\nabla}/K_0$. The dimensional variables and operators are accented; g_0, c_0 are density and speed of sound in reference medium respectively (in our case - volume dominant reference). It means that $c = 1$ and $g = 1$ for reference medium. The characteristic wave number K_0 and pulsation ω_0 are restricted by the relation: $K_0 c_0 = \omega_0$. $\omega_0 \equiv 2\pi/T_0$, where T_0 is reference time (e.g. Time window). In homogeneous regions of the medium $a(n) = a(\mathbf{x},n)$; $a(\mathbf{x},n)$ denotes spatial distribution of the small signal coefficient of absorption, $a_0(n)$ is the absorption coefficient of the reference medium.

We assume that reference homogeneous medium surrounds L regions υ_l of space. The regions are bounded by surfaces s_l $l = 1,...,L$. Each region υ_l is filled with homogeneous medium and its normalized density $g_l \neq 1$, as well as normalized speed of the longitudinal waves $c_l \neq 1$. The multiple-theory sum of the υ_l sets describes the structure being submerged in reference medium. Thus spatial distributions of sound speed, density and absorption coefficient have a form:

$$
\begin{aligned}
c(\mathbf{x})^2 &= 1+\sum_l \mathrm{d}c_l(\mathbf{x})^2 = 1+\sum_l \chi_l(c_l{}^2-1)\\
g(\mathbf{x}) &= 1+\sum_l \mathrm{d}g_l(\mathbf{x}) = 1+\sum_l \chi_l(g_l-1)\\
a(\mathbf{x},n) &= a_0(n)+\sum_l \mathrm{d}a_l(\mathbf{x},n) = a_0(n)+\sum_l \chi_l(a_l(n)-a_0(n))
\end{aligned}
\tag{2}
$$

where d… denotes step rise of material parameters; $\chi_l \equiv \chi(\upsilon_l)$ is the characteristic function of υ_l, χ=1 for $\mathbf{x}\in\upsilon_l$, $\chi=0$ for $\mathbf{x}\notin\upsilon_l$, $\chi=1/2$ for $\mathbf{x}\in s_l$. For V and **Q**, we heave

$$
\begin{aligned}
\mathrm{V} &= \sum_l \chi_l n^2\left(\frac{1}{1-2i(a_0(n)/n)}-\frac{1}{c_l{}^2\left(1-2i(a_l(n)/g_l c_l^2\, n)\right)}\right)\\
\mathbf{Q}(\mathbf{x}) &= \mathrm{Q}\mathbf{e}(\mathbf{x})\delta(\mathrm{s}) = \left(\sum_l \sigma_l\left(\frac{1-g_l}{(g_l+1)/2}\right)\right)\mathbf{e}(\mathbf{x})\delta(s)
\end{aligned}
\tag{3}
$$

Vector $\mathbf{e}_l(\mathbf{x})$ is externally normal to s_l in $\mathbf{x}\in s_l$ and is unit. Because $\mathbf{e}(\mathbf{x})=\{\mathbf{e}_l(\mathbf{x}):\mathbf{e}_l\perp s_l, l=1,...,L\}$ is a general field of the unit vectors being normal to the structure.

For the assumed model of structure of medium the Eq. (1) was transformed into set of the integral equations [8] that describe scattering on potentials V and Q of the structure.

$$
\begin{aligned}
C(\mathbf{x}) = C^0(\mathbf{x}) &- \int_\upsilon G(r(\mathbf{x},\mathbf{x}'))\mathrm{V}(\mathbf{x}')C(\mathbf{x}')d\upsilon\\
&- \int_s G(r(\mathbf{x},\mathbf{x}'))\mathrm{Q}(\mathbf{x}')B(\mathbf{x}')ds
\end{aligned}
\tag{4}
$$

$$
\begin{aligned}
B(\mathbf{x}) = B^0(\mathbf{x}) &- \int_\upsilon \partial G(r(\mathbf{x},\mathbf{x}'))\mathrm{V}(\mathbf{x}')C(\mathbf{x}')d\upsilon\\
&- \int_s \partial G(r(\mathbf{x},\mathbf{x}'))\mathrm{Q}(\mathbf{x}')B(\mathbf{x}')ds
\end{aligned}
\tag{5}
$$

where $G(r,n)\equiv\exp(ik(n)r/4\pi r)$, $r=r(\mathbf{x},\mathbf{x}')=|\mathbf{x}-\mathbf{x}'|$, $C^0(\mathbf{x})\equiv C^0(\mathbf{x},n)$ is a solution of Helmholtz equation in reference medium (incident field), $G(r(\mathbf{x},\mathbf{x}'))=G(r(\mathbf{x},\mathbf{x}'),n)$ is the Green function of the Helmholtz equation, $B^0\equiv\mathbf{e}\cdot\nabla C^0$, $B(\mathbf{x},n)\equiv\mathbf{e}(\mathbf{x})\cdot\nabla C(\mathbf{x},n)$, $\partial G(r)\equiv\mathbf{e}(\mathbf{x})\cdot\mathbf{e}(\mathbf{r})\partial_r G$, $\mathbf{e}(\mathbf{r})=\nabla r=\mathbf{r}/r$. We solve the Eqs. 4, 5 numerically. The developed solver enables to find the solution $E\equiv\left[C-C^0;B-B^0\right]$ – scattered field in the form

$$
E(\mathbf{x},n)=\sum_{j=1}^{J}E^j(\mathbf{x},n)=\sum_{j=1}^{J}\bigcup_{m=1}^{M}\sum_{l\in Lm}E_l^j(\mathbf{x},n)
\tag{6}
$$

where indices *j* = 1,2,3… number the orders of scattering, index *m* numbers the scattering substructures of the full structure. *Lm* denotes the set of the indices of the elements

constituting the *m*-th substructure. The sequence of the summation in Eq. (6) may be changed. That means that the solver enables the multi-scattering decomposition of scattered field with respect to the contributions from substructures taking into account the backscatter coefficients in successive (I,II,III) orders of the scattering. The results of the structural analysis of the field scattered on complex structures (also random), e.g trabecular will be presented later.

2. TRABECULAR BONE MODEL

The skeleton of the model of trabecular bone structure, applied in scattering field calculations, is presented in Figure 1: (a) left. One of skeleton structures parallel to the *x-z* plane (horizontal in respect to the incident field) is shown in Figure 1: (a) right. The cylinder with diameter Φ and length d was adopted as the model of trabecula and bar. Each segment of the skeleton is the axis of cylinder. The skeleton was obtained randomly (see. [5]). By the variation of the probability distribution functions and their parameters we can create different statistical properties of the physical and geometrical parameters of the structure. The structure is immersed in absorbing fluid filer.

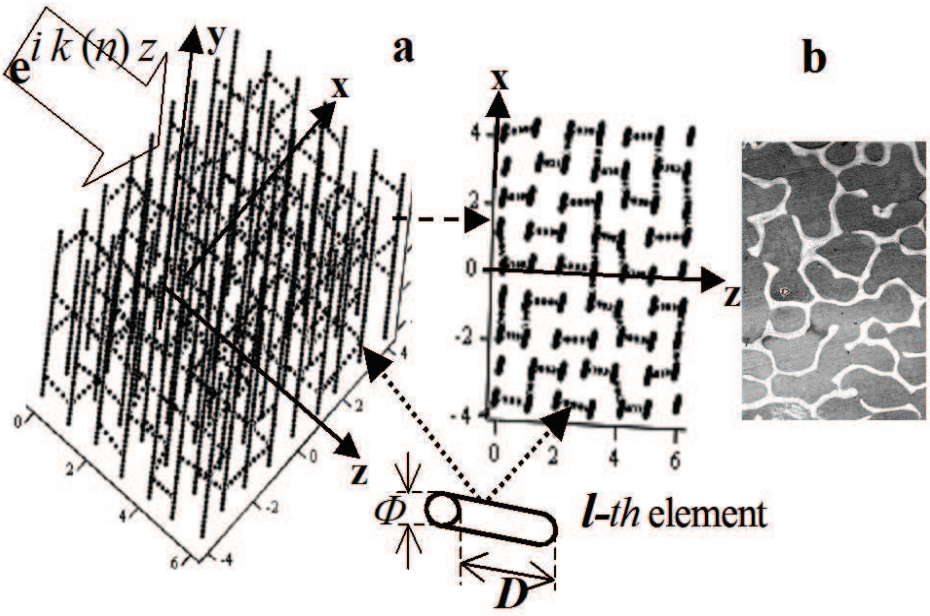

Fig 1. (a) left: full skeleton of the trabecular bone model; right: one of horizontal substructures in the skeleton; (b) the cross-section of the real trabecular bone structure

3. RESULTS OF THE EXACT MODEL

At the beginning the regular structure was constructed of the cuboids of dimensions 2 mm in the **y** direction and 1×1 mm in the **x** and **z** directions. For the nodes displacement the uniform probability was assumed in range (–0.15; 0.15) mm. Also uniform probability for elimination of some elements from the structure were used. Values of sound speed and densities (4000 m/s and 2000 kg/m^3 with ±5% standard deviation) of each trabecula were selected basing on Gamma distribution. For trabeculae, in *y* direction and in horizontal planes, mean values Φ = 0.1 and 0.08 mm with deviations ±20% and ±25% respectively, were assumed. For surrounding medium (marrow) as well as surrounding space g_0 = 1000kg/m^3,

c_0=1500m/s. The absorption parameters for fluid filer was α_1= (0.23;1.15;2.3)·10^{-4} Np/mHz, $a(n) = \alpha_1 c_0 |n| / 2\pi$. Total number of elements (trabeculae) was 443. Total dimensions are: [–4;4] mm in *x*, [–4;4] mm in *y*, [0;6] mm in *z* direction (384 mm^3).

The unit plane wave was assumed as the incident field $C^0 = \exp(ik(\nu)z)$ $z \geq 0, \nu \in [0.5, 3]$ MHz with step 0.0333 MHz. Dimensionless frequency is $n = 15,16,...,90$.

3.1 SCATTERING FIELD DISTRIBUTIONS

Exemplary distributions of scattering fields for the absorption parameter $\alpha_1 = 2.3 \cdot 10^4$ in subsequent orders of scattering and for the selected frequencies are shown in Fig 2.

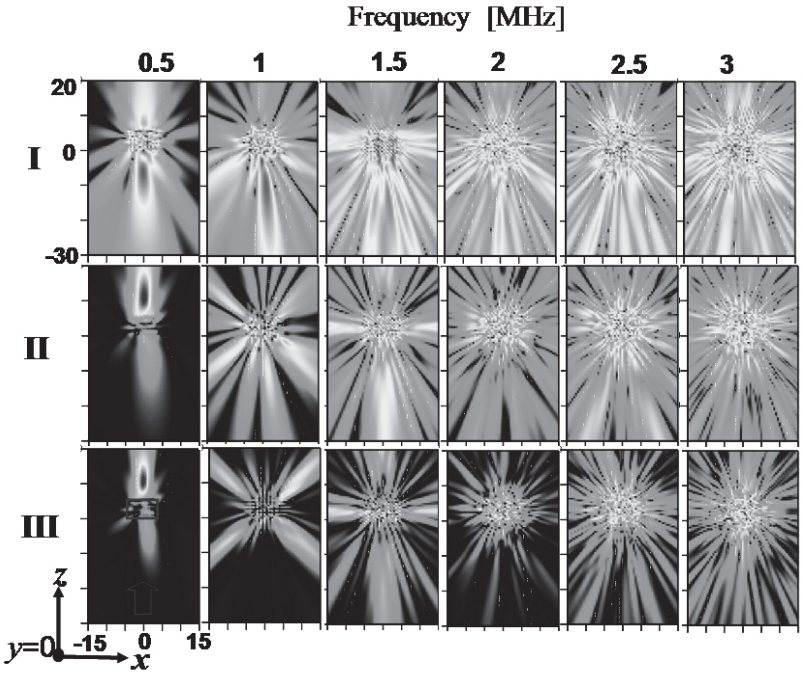

Fig. 2. Distributions of fields in subsequent orders of scattering in rows: I, II, III, while in function of frequency from 0.5 MHz to 3 MHz they are shown in columns. The axis are in mm

Grey scale refers to the logarithmic scale of values. Contour of the scattering structure and its location is shown by white rectangle whereas white narrow indicates direction of incident wave.

3.2 BACKSCATTER COEFFICIENTS

We define substructures: horizontal (denoted by '**h**') as a set of all trabeculae that are situated in planes being parallel to the *x*-*z* plane, and vertical (denoted by '**y**') as a set of all trabeculae which are parallel to the **y** axis.

In Figure 3 **S**$_{\mathbf{I}}$, **S**$_{\mathbf{II}}$ and **S**$_{\mathbf{III}}$ are the BECS coefficients, that were obtained in subsequent orders of scattering (first-I, second-II, third-III) and in function of frequency ν . The influence of the absorption of the fluid filer on the effective cross-section in each order is presented. The plot p1 correspond to the last α_1=0.23·10^{-4}, p2 to the middle α_1=1.15·10^{-4} and p3 to the α_1=2.3·10^{-4} value of absorption parameter. Square roots $\sqrt{\mathbf{S_I}}$, $\sqrt{\mathbf{S_{II}}}$, $\sqrt{\mathbf{S_{III}}}$ were applied for

better representation. Moreover, the square root from the effective cross-section is a proper norm of the signal received by transducer placed close to the scatter.

In Figure 4. the contribution of substructures **y** and **h** to backscatter effective cross-sections for the case p1 in subsequent orders of scattering is presented.

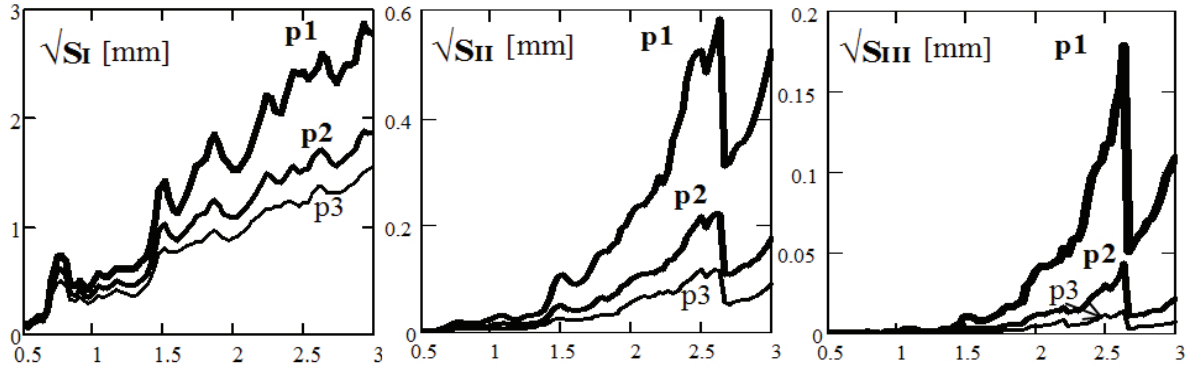

Fig. 3. BECS decomposition in respect to scattering order, first- SI, second-SII and third-SIII. Plots p1, p2, p3 corresponds to the low-p1, middle-p2 and extreme-p3 value of absorption parameter. Frequency in MHz

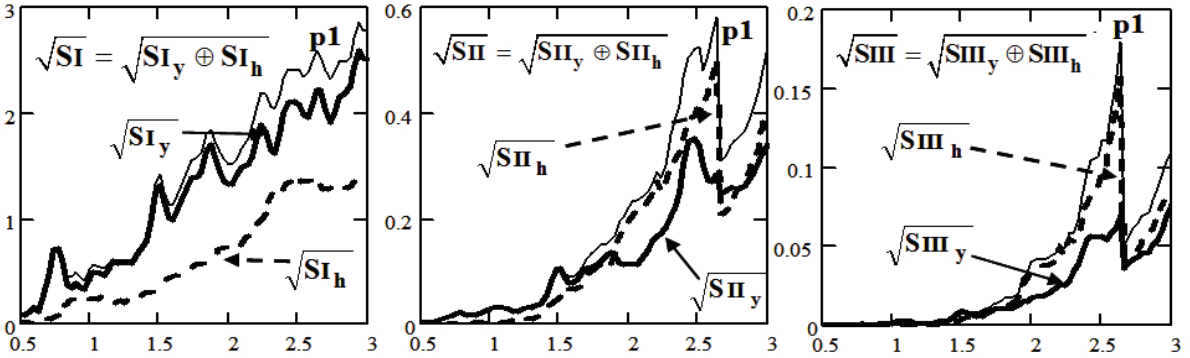

Fig. 4. Contribution of substructures **h** and **y** in subsequent orders of scattering as well as in respect to frequency (in MHz) for the case p1 of the absorption parameter

In the numerical calculations the $\mathbf{SI_y}$, $\mathbf{SI_h}$ and $\mathbf{SI=SIy \oplus SIh}$ – BECSs for the fields scattered on the substructures **y** and **h** subsequently and total BECS in the I-st order of scattering were determined separately. The same procedure was applied for higher orders of scatering (II, III). The symbol $\oplus$ denotes summation with interferences of the fields scattered by diferent substructures. However $\oplus \cong +$ – ordinary summation of the scattered powers.

4. PROBLEM FORMULATION

In Fig. 3 we observe several peaks in the run of $\sqrt{\mathbf{SI}}$ plots. Some of them are repeated in the same positions in higher order of scattering. In description of the multi-scattering process $\mathbf{S = SI \oplus SII \oplus SIII}$ the component **SI** is dominate and the field scattered in the I-st order impacts the results in higher order. Then we restrict our investigations to the 'peaks' phenomenon in the I-st order of scattering and they bases on the $\sqrt{\mathbf{SI}}$ properties. In Fig. 5 the above mentioned peaks are marked by vertical dashed arrows.

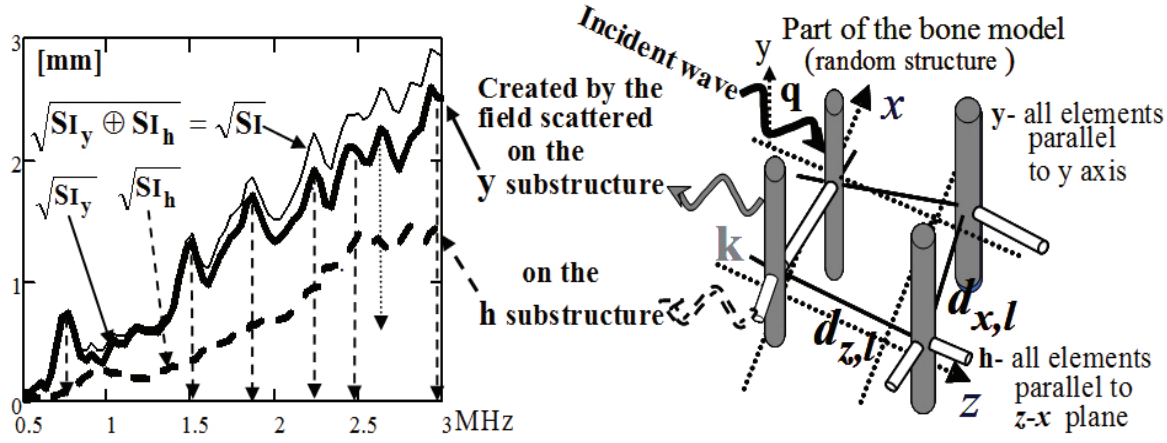

Fig. 5. Structural analysis of the scattered fields. Diagram of contributions of the selected substructures **y**, **h** in creation of the **SI** – I-st order BECS

The scattering on the random structure is a stochastic process. Therefore we ask: Are the marked frequencies and the peaks in Fig. 5 are specific or accidental (randomly distributed) for the scattering structure and scattering process? Do the marked peaks change the position if the distribution of the model parameters (elements position) change?

We have found by numerical calculations – for other sets of random parameters of the bone model – that some one of them may disappear. However, if they remain then they occur for the same frequency if the averages of the spatial distributions of the element positions in the structure are the same.

Fig. 5 shows participations of the selected substructures **y** and **h** in the creation of the field scattered in the I-st order. However the fields scattered by **y** and **h** structures are comparable (in the norm with factor ~0.5) the contribution of the field scattered on **h** structure to the $\sqrt{\mathbf{SI}}$ is smooth and over eight times smaller then contributions from **y** substructure.

The vertical structure **y** is dominating and only this structure forms the peaks that will be taken into consideration. This observation enables to create a simplified (averaging) analytical model.

5. SIMPLIFIED MODEL AND PROBLEM SOLUTION

Performance: (1) eliminating **h** substructure (interconnections), (2) averaging geometrical and material parameters of the **y**-structure elements (vertical trabeculae), (3) averaging the distances $d_{z,l}$, $d_{x,l}$ between subsequent elements along z and x axes

$$d_x = \left\langle d_{x,l} \right\rangle_l = d = \left\langle d_{z,l} \right\rangle_l = d_z \tag{7}$$

and, (4) applying *Neumann-Born* approximation in calculation of the scattered field; we obtain, simplified regular structure like crystal with cubical elementary cells and square lattice parallel to z-x plane with lattice constant $d_z = d_x = d = 1$ mm and analytical description of the scattered field – see Fig. 6.

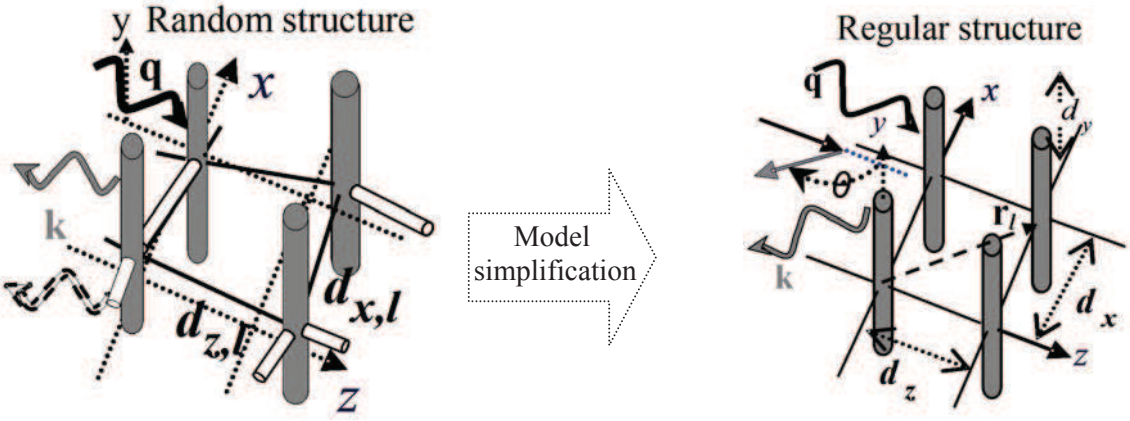

Fig. 6. Model simplification: left – full bone model (random); right – simplified model (regular), $d_z = d_x = d = 1$ mm

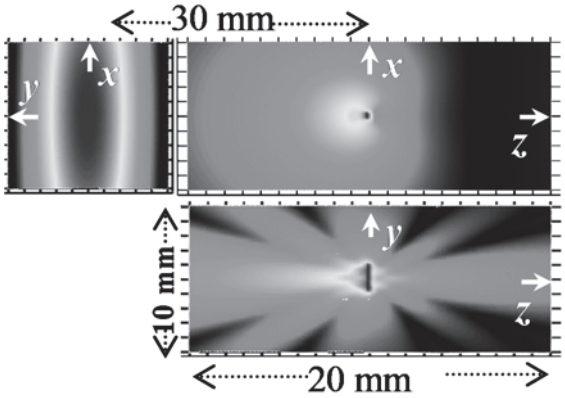

Fig. 7. Example of the spatial field distribution of the field scattered on the single element with $D = 2$ mm and $\Phi = 0.1$ mm; Incident field – single plane wave with $\nu = 1.875$ MHz

For determination of the $C(\mathbf{r},\nu)$ – total field scattered in the simplified bone model we apply methods commonly used in the summation of the properties of the individual elements creating regular multi-element structures – especially methods used in crystallography. Neglecting detailed discussion we obtain

$$C\left(\mathbf{r}(\theta,\varphi),\nu\right)=\sum_{l=1}^{L} Cs\left(\mathbf{r}(\theta,\varphi),\nu\right)\mathrm{e}^{i(\mathbf{k}-\mathbf{q})\cdot\mathbf{r}_l}=Cs\left(\mathbf{r}(\theta,\varphi),\nu\right)\cdot\prod_{j=z,x,y}\frac{\sin\left(0.5L_j d_j\left[\mathbf{k}-\mathbf{q}\right]_j\right)}{\sin\left(0.5 d_j\left[\mathbf{k}-\mathbf{q}\right]_j\right)} \quad (8)$$

where $Cs(*)$ – spatial distribution of the field scattered on the single element (Fig. 7), $\mathbf{r}(\theta,\varphi)$ – is the vector of the space Cartesian coordinates expressed by spherical coordinates. The angle θ is measured respect z axes (θ,φ – scattering angles). $\mathbf{r}_l \equiv \mathbf{r}_s + \left(\mathbf{e}_z d\cdot l_z + \mathbf{e}_x d\cdot l_z + \mathbf{e}_y d_y\cdot l_y\right)$ is the vector coordinates of the lattice nodes (in our case $lz = 0,\ldots,Lz - 1 = 6$, ; $lx = 0,..,\ Lx - 1 = 8$; $ly = 0,..,\ Ly - 1 = 3$), $\mathbf{q}$ is the wave vector of the incident wave**,** $\mathbf{k}$ is the wave vector of the scattered wave, ν is the frequency.

The magnitudes of the interference amplifications of the scattered fields are described by the last factor in Eq. 8. The analyzis leads to the conclusion that the main directions and frequencies of the interference amplification are determined by the equations (*Laue* [3])

$$\mathbf{k}-\mathbf{q}=\mathbf{w}\equiv 2\pi\left(\mathbf{1_z}\frac{m}{d}+\mathbf{1_x}\frac{l}{d}+\left(\mathbf{1_y}\frac{s}{d_y}\right)\right) \qquad m,\ l,\ s-\text{integer} \tag{9}$$

$$|\mathbf{k}|=|\mathbf{q}|=k=2\pi\nu/c_0 \qquad \textit{(elastic scattering)}$$

where $\mathbf{1_z},\mathbf{1_x},\mathbf{1_y}$ are unit vectors from inverse lattice in the Fourier space. The Fig. 8 gives geometrical interpretation of Eq. 9 and the vectors **w.**

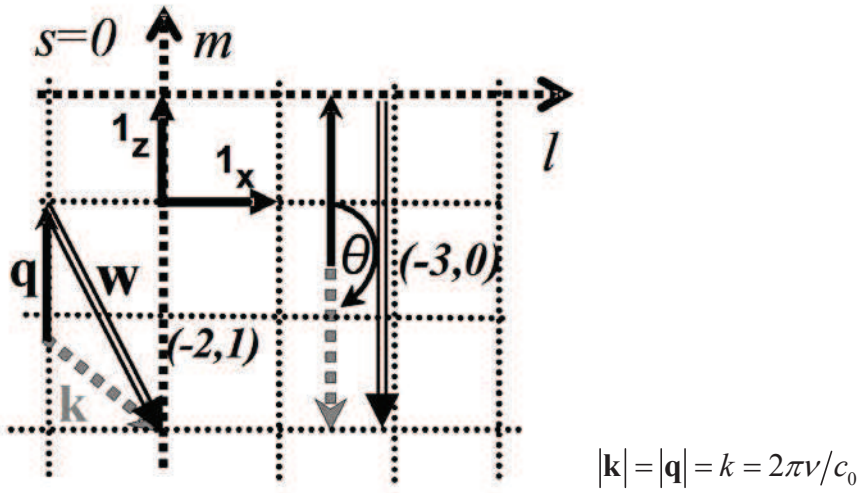

Fig. 8. Ewald construction-geometrical interpretation of Eq. 9 for elastic scattering. Examples of the two permissible scattering vectors **k**

Accordingly to the relative configuration determined by the incident plane waves (along *z* axes) and space orientation of the model lattice (Figs 1 and 6 Right) the set of Eq. 8 can be written as

$$\mathbf{k}=k\begin{pmatrix}\cos(\theta)\\ \sin(\theta)\cos(\varphi)\\ \sin(\theta)\sin(\varphi)\end{pmatrix},\ \mathbf{q}=k\begin{pmatrix}1\\0\\0\end{pmatrix};\quad \begin{aligned}k\left(\cos(\theta)-1\right)&=m\left(2\pi/d\right)\\ k\sin(\theta)\cos(\varphi)&=l\left(2\pi/d\right)\\ k\sin(\theta)\sin(\varphi)&=s\left(2\pi/d_y\right)\end{aligned},\quad k=\left(2\pi\nu/c_0\right) \tag{10}$$

and resolve respect ***ν***. We obtain the main frequencies of the interference amplification of the backs scatered fields (alsso transmited),

$$\nu_{m,l,s}=\frac{c_0}{2d}\frac{-1}{m}\left(m^2+l^2+\left(\tfrac{d}{d_y}\right)^2 s^2\right),\ \textit{it must be}\ \ m\le 0 \tag{11}$$

The cases $m < 0$ corresponds to the backscattering. For $m = 0$ it mast be $\theta = 0$, $l = s = 0$ (**k = q**) we obtain forward scattering-transmission. The last factor in Eq. 8 don't modulate the frequency dependent scattering coefficients. They are determined by the single element scattering properties (field *Cs*(ν).

Using formula Eq. 8 we determined $\mathbf{SI}_{Si}$ – BECS for simplified model (with absorption). The $\sqrt{\mathbf{SI}_{Si}}$ plot is shown on Fig. 9 (left down). The positions of their frequencies peaks given by Eq.11 are collected in matrices on Fig. 9 (right).

As we see the simplified bone model very good predicts and explains (except for frequency 2.67 MHz marked by?) the positions of the peaks occurring in the exact random model – $\sqrt{\mathbf{SI}}$ plot on Fig. 9 (left up).

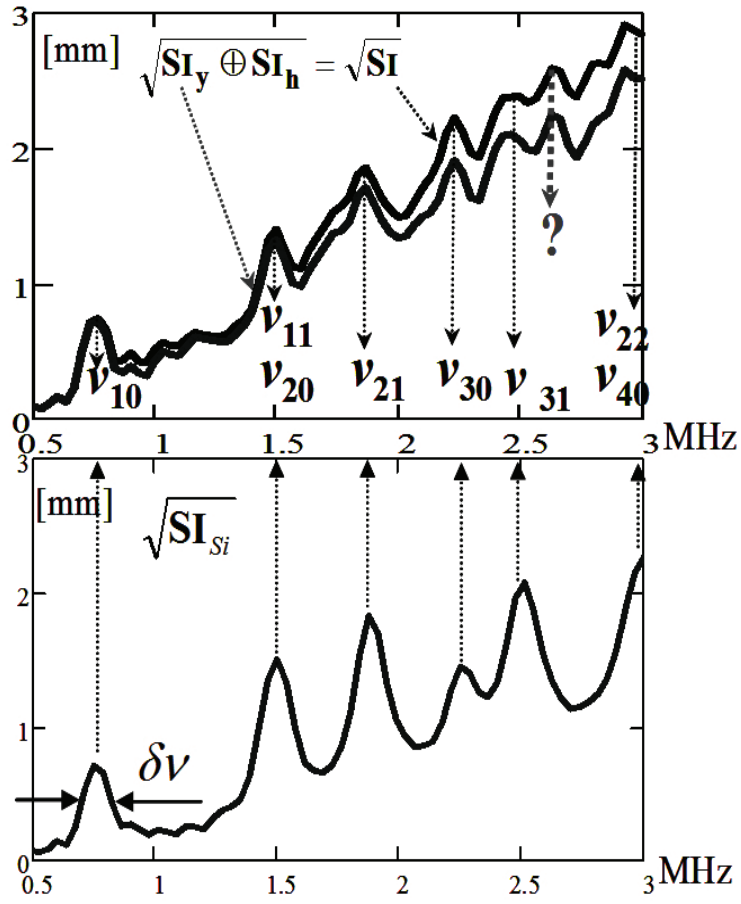

$\nu_{m,l,0} =$

m \ l	0	1	2
1	0.75	1.5	3.75
2	1.5	1.875	3
3	2.25	2.5	3.25
4	3	3.188	3.75

The scattering line width $\delta\nu$ is inversely proportional to the model dimensions – number of elements in the scattering directions for given frequency $\boldsymbol{\nu}_{m,l}$

Fig. 9. Comparison of the models results. Explanation of the frequency peeks positions occurring in exact random model – **SI**(*ν*), on the basis of the results of simplified (crystallographic) model $\mathbf{SI}_{Si}(\nu)$

6. COMPARISON WITH EXPERIMENT

The experimental data was copied from the paper presented in JASA [6].

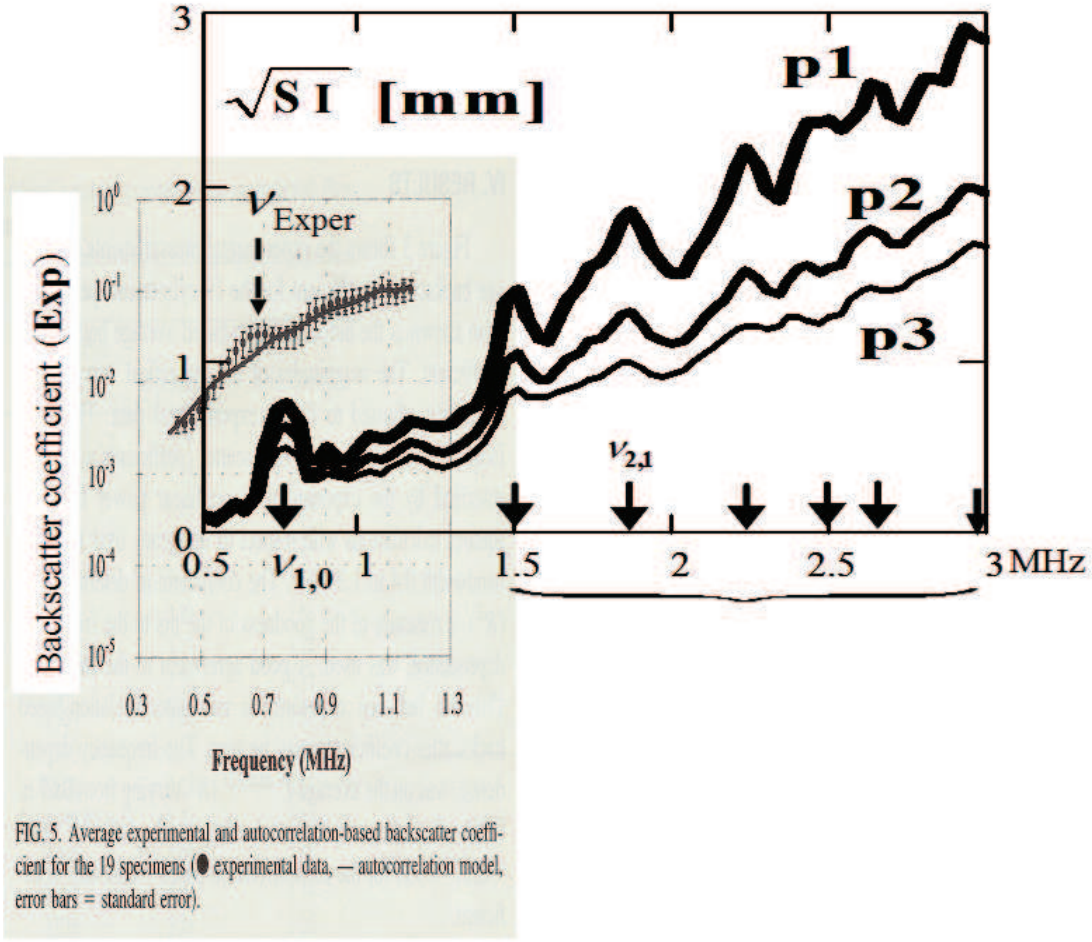

Fig. 10. The juxtaposition of the experimental results – gray rectangle, with the results of the full random bone model. The frequency axes are the same for both presentations

For both presentation we rewrite below descriptions of the experimental results:

• Average experimental – based backscatter coefficient for the 19 specimens;
– Autocorrelation model (error bars = standard error).

The experimental spectral line (around ν_{Exper}) in the linear value scale is more clear and similar to the spectral line (around $\nu_{1,0}$) obtained in theoretical or numerical models of the bone scattering.

There was no experimental data in the higher frequency band. Also the probe diameter in the currently applied experiment configurations was to small for the detection of some frequencies e.g. ν_{21}.

On the basis of the presented theoretical results we conclude that corresponding to the experimental peak at frequency ν_{Exper} the experimentally equivalent 'lattice constant' – or more precisely speaking-mean distance between long trabeculae is equal d_{Exp} = 1.07 mm, while in our models d = 1 mm.

7. CONCLUSIONS

The developed algorithm enables the analysis of the scattering field characteristics taking into account not only the scattering order but also the specific influence and validity of the

scattered substructures. The examples of utilization of this algorithm has been presented for trabecular bone model. Namely – the simplified analytical model corresponding to the models used in the description of crystals was presented and justified.

In the description of the location of frequency peaks that are specific for the scattering the simplified – averaging – analytical model is consistent (highly correlated) with the results of the exact model of the random structure (except peaks 2.67 MHz).

Random structures can have or preserve properties of regular structures or some of their average characteristics (e.g. distances between elements, number of elements) that can be determined by correlating them with models of regular structures.

In the range of frequencies and sizes of the probes which were used in the investigation of bones a good agreement of the model predictions with the experimental results was obtained (for the given example the interpretation of the experiment on the basis of models shows that $<d_{Exp}> = 1.07$ mm).

ACKNOWLEDGMENTS

This work is supported by Ministry of Science and Higher Education (grant N N518 426936, N N518 503339)

REFERENCES

[1] Wear K., Ultrasonic Scattering from Cancellous Bone: A review, IEEE Trans. Ultrason. Freq. Contr., Vol. 55, No 7, (2008), 1432–1441.

[2] Hosokawa A., Development of Numerical Cancellous Bone Model for Finite-Difference Time-Domain Simulations of Ultrasound Propagation, IEEE Trans. Ultrason. Freq. Contr., Vol. 55, No 6, (2008), 1219–1233.

[3] Kittel C., Introduction to solid state physics, John Wiley & Sons, Inc, New York 1966.

[4] Brekhovskikh L. M., Godin O. A., Acoustics of Layered Media I, Springer, Verlag – Berlin – Haidelberg – New York 1990, pp. 1–14.

[5] Wojcik J., Litniewski J., Nowicki A., Example of structure modeling and analysis of ultrasound scattering for trabecular bone, Archives of Acoustics, 2010, 701–713.

[6] Chaffai S., Roberjot V., Peyrin F., Berger G., Laugier P., Frequency dependence of ultrasonic backscattering in cancellous bone: Autocorrelation model and experimental results, J. Acoust. Soc. Am., 108, 5, (2000), 2403–2411.